Simulating Thioflavin T and Congo Red Binding to the Fibril Structure of Amyloid- β (1-42)

B. Frieg, H. Gohlke

published in

NIC Symposium 2020

M. Müller, K. Binder, A. Trautmann (Editors)

Forschungszentrum Jülich GmbH, John von Neumann Institute for Computing (NIC), Schriften des Forschungszentrums Jülich, NIC Series, Vol. 50, ISBN 978-3-95806-443-0, pp. 53. http://hdl.handle.net/2128/24435

© 2020 by Forschungszentrum Jülich

Permission to make digital or hard copies of portions of this work for personal or classroom use is granted provided that the copies are not made or distributed for profit or commercial advantage and that copies bear this notice and the full citation on the first page. To copy otherwise requires prior specific permission by the publisher mentioned above.

Simulating Thioflavin T and Congo Red Binding to the Fibril Structure of Amyloid-β(1-42)

Benedikt Frieg¹ and Holger Gohlke^{1,2}

¹ John von Neumann Institute for Computing (NIC), Jülich Supercomputing Centre (JSC) and Institute for Complex Systems - Structural Biochemistry (ICS-6), Forschungszentrum Jülich, 52425 Jülich, Germany

E-mail: {b.frieg, h.gohlke}@fz-juelich.de

² Institute for Pharmaceutical and Medicinal Chemistry, Heinrich Heine University Düsseldorf, 40225 Düsseldorf, Germany *E-mail: gohlke@hhu.de*

Binding modes for two amyloid- β (1-42) fibril tracers, namely Thioflavin T and Congo red, were identified using unbiased all-atom molecular dynamics simulations and binding free-energy computations. Both dyes bind to primarily hydrophobic grooves on the amyloid fibril surface, perpendicular to its β -strands. Binding affinities computed by the MM-GBSA method are in excellent agreement with experimental values and corroborate the proposed binding modes. The binding modes can guide the rational design of novel biomarkers for amyloid fibrils.

1 Introduction

Alzheimer's disease (AD) is a progressive, unremitting, neurodegenerative disorder, and the leading cause of dementia.^{1–4} In 2018 it was estimated that more than 50 Mio. people in the world are living with dementia, with two-thirds associated with AD.^{5,6} There is a new dementia patient around the world every three seconds, and it is estimated that by 2030 more than 80 Mio. will be diagnosed with dementia.⁶ The considerable number of dementia patients is directly associated with the healthcare system facing high costs, and it is estimated that the costs will rise to worldwide \$2 trillion by 2030.⁶ Thus, dementia and AD, in particular, are significant challenges for the modern healthcare system.

Since 1998, more than 100 drug candidates have been tested, but only four have been approved for therapeutic applications in AD.^{5, 6} The authorised drugs, however, only help to manage some of the symptoms but do neither stop nor slow the progression.^{5, 6} Thus, currently, there is no cure for AD, and considering the underlying pathologic causes of AD, there is not going to be a cure in near future.^{5, 6}

The AD type of dementia has been related to an imbalance between the production and elimination of the protein fragment amyloid-beta $(A\beta)$.⁷ Accumulation of $A\beta$ outside of the nerve cells (neurons) is associated with cell death in AD.^{5,6} The consequence is that neurons essential for cognitive function are damaged or destroyed and, because AD is a progressive disease, more and more neurons will be destroyed over time.^{5,6}

Currently, there is no test available that conclusively diagnoses AD. Diagnostic strategies focus on multiple tools and aspects, such as detecting key biomarkers for AD.^{5, 6} For AD, the accumulation of A β has been recognised as a biomarker.^{5, 6} As changes in the brain begin 20 years or more before any AD-related symptoms are expected to occur,⁸ a conclusive test for AD-related biomarkers will be essential. This is all the more so as a

therapeutic intervention in the very early stages is currently considered necessary to slow or stop the progression of AD.^{5,6}

Under high concentration, $A\beta$ peptides can aggregate to more senior oligomeric complexes or arrange to symmetric and periodic fibrils, which denote pathological hallmarks in AD.^{4,7,9,10} Thus, molecular probes that detect amyloid fibrils *in vitro* or *in vivo*, such as Thioflavin T (THT, Fig. 1A) and Congo red (CGR, Fig. 1B),^{11,12} are essential for an accurate and conclusive diagnosis of amyloid fibrils-related diseases. THT and CGR are potent fluorescent dyes that form fluorescent complexes with amyloid and amyloid-like fibrils.^{13–15} For both probes, previous studies suggested binding modes,^{11,12,16} but the exact nature of how both probes bind to the AD-related A β (1-42) fibril remained elusive. Such knowledge is, however, essential for the rational search for novel molecular probes.^{11,12}

Recently, the first high-resolution structure of the $A\beta(1-42)$ fibril was obtained by cryoelectron microscopy and nuclear magnetic resonance spectroscopy, ¹⁷ opening up the possibility to predict the binding modes of THT and CGR at the atomistic level. Here, we used molecular dynamics (MD) simulations of free diffusion of THT and CGR in the presence of the $A\beta(1-42)$ fibril to derive such binding mode models. The probes were not biased throughout the binding process by any prior knowledge of the binding epitopes. That way, the probes spontaneously recognise energetically preferred binding epitopes, yielding binding mode models that are in agreement with previous observables.

Figure 1. Structures of amyloid biomarkers. Structure of Thioflavin-T (THT, A) and Congo red (CGR, B) with protonation states according to pH 2.

2 Methods

System preparation and molecular dynamics simulations

To investigate THT and CGR binding to the $A\beta(1\text{-}42)$ fibril (PDB ID 5OQV^{17}), we performed unbiased MD simulations. The protonation states of all residues of the fibril at pH 2 were resolved by NMR spectroscopy and incorporated in our setup. That way, the protonation states in the simulations match those in *in vitro* experiments. THT and CGR were also prepared for pH 2 using Epik^{18, 19} (Fig. 1). We randomly placed one dye molecule and the $A\beta(1\text{-}42)$ fibril structure into an octahedral box using PACKMOL,²⁰ and neutralised and solvated the systems with chloride atoms and TIP3P²¹ water, respectively. For both dyes, we prepared 45 different initial configurations, in which the distance between the dye molecule and the $A\beta(1\text{-}42)$ fibril ranged from 13 Å to 62 Å. The systems were

subjected to production simulations of 1 μ s length each, to study THT and CGR binding to the A β (1-42) fibril. The minimisation, thermalisation, and equilibration protocol is reported in Ref. 23, which was already applied previously to study ligand binding processes. All minimisation, equilibration, and production simulations were performed with the *pmemd.cuda* module^{26, 27} of Amber16²² on JUWELS.

During visual inspection of the MD trajectories, we observed multiple binding and unbinding events of the dye molecules to and from the A β (1-42) fibril (the workflow is exemplarily shown for THT in Fig. 2). We determined all stably bound dye poses by calculating the Root Mean Square Deviation (RMSD) of the dyes after superimposing the A β (1-42) fibril structure. That way the RMSD becomes a measure for the spatial displacement of a dye molecule between two snapshots. THT poses with RMSD < 1.2 Å and CGR poses with RMSD < 1.5 Å, respectively, were defined as stably bound. The stably bound poses were subjected to hierarchical clustering, using the minimum distance between the clusters as cluster criterion. Starting from ϵ = 2.0 Å, we gradually increased ϵ in 0.5 Å intervals until the population of the largest cluster remained unchanged (ϵ _{THT} = 5.0 Å and ϵ _{CGR} = 4.5 Å).

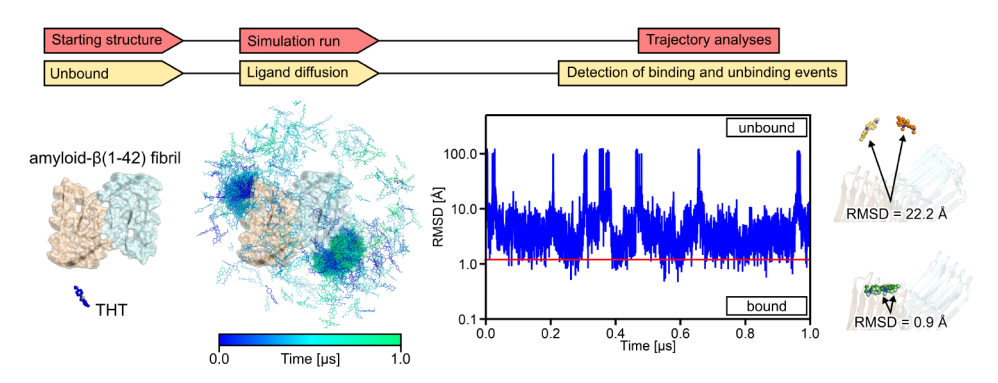


Figure 2. Schematic workflow to identify a binding mode from an MD simulation of ligand binding. From left to right: In the starting configuration, the $A\beta(1\text{-}42)$ fibril structure (cartoon-surface representation) and Thioflavin-T (THT, sphere model) are spatially separated. During MD simulations of ligand binding, the $A\beta(1\text{-}42)$ fibril and THT molecules diffuse freely and without guiding force (only the diffusion of the THT is shown for clarity purposes). The THT diffusion (shown as stick models) is coloured according to the simulation time (see the colour range). The resulting trajectory is analysed with respect to THT binding to or unbinding from the $A\beta(1\text{-}42)$ fibril. In this study, the RMSD between two consecutive THT conformations, after superimposing the fibril, was used to characterise the (un-)binding events. The larger the RMSD, the larger is the spatial displacement between two consecutive THT conformations, as indicated on the right. In this example, THT is considered stably bound, if the RMSD < 1.2 Å (indicated by the red line).

Molecular mechanics generalised Boltzmann surface area (MM-GBSA) calculations

The most-populated clusters were further investigated by binding free energy calculations, performed with MMPBSA.py, 22,29 yielding ΔG_{bind} . We obtained the standard free energy of binding ΔG_{bind}^0 for a standard state of 1 M, 32 which is directly related to the dissociation constant $K_{\rm D}$ according to Eq. (1)

$$\Delta G_{bind}^0 = RT \ln(K_D) \tag{1}$$

where R is the universal gas constant ($R = 0.001987 \text{ kcal K}^{-1} \text{ mol}^{-1}$), and T = 300 K.

3 Results

Unbiased MD simulations of THT and CGR binding to the A β (1-42) fibril and subsequent binding free energy calculations were applied to determine the binding epitope and a binding mode in full atomic resolution for both probes.

During MD simulations of THT and CGR binding, we observed multiple binding and unbinding events of the dyes to and from the $A\beta(1-42)$ fibril structure. The unbinding events are more likely in the case of THT, suggesting that THT binds weaker to the $A\beta(1-42)$ fibril structure than CGR. To identify the binding epitopes of THT and CGR, we focused our analyses on the bound probe conformations. As to THT, stable bound structures were predominant around amino acids V18, F20, and E22. Due to the symmetric organisation of the $A\beta(1-42)$ fibril, high THT concentrations are observed at both protofibrils (Fig. 3A). As to CGR, by contrast, the stably bound poses are distributed across the complete $A\beta(1-42)$ fibril surface (Fig. 3B), and CGR conformations parallel and perpendicular to the fibril axes are observed. In contrast to THT, the area around V18, F20, and E22 is less populated by CGR molecules, suggesting that both probes most likely bind to two distinct epitopes.

To extract the predominant binding pose from all stable bound conformations of THT and CGR, all structures shown in Fig. 3A + B were subjected to hierarchical clustering. The ten most populated clusters were further subjected to binding free energy calculations, yielding a dissociation constant K_D^{comp} (Eq. (1)) for each cluster. Based on both the cluster populations and K_D^{comp} , we extracted a binding mode model for either probe, which revealed several interesting facts.

As to THT, the largest cluster contains 11% of all considered configurations and also shows the most favourable binding affinities. The THT conformations in this cluster bind to V18, F20, and E22, such that the protonated amino function of THT is stabilised by a hydrogen bond interaction with E22, while the aromatic moieties of THT interact with F20 and V18 (Fig. 3C). Interestingly, the side chains of F20 adapt a V-shaped orientation, such that the phenyl rings in F20 align almost parallel to the aromatic rings in THT, forming π - π -stacking interactions. THT binds across four layers of A β (1-42) peptides with its axis oriented almost perpendicular to the orientation of the stacked β -strands of the A β (1-42) fibril. The observation that multiple segments are essential for THT binding also provides an explanation why THT recognises fibrillary structures, but no single $A\beta(1-42)$ peptides. For the reported binding mode, $\Delta G_{bind}^0 = -9.06$ kcal mol⁻¹, yielding $K_D^{comp} = 251.21$ nM, which is in agreement with experimentally derived binding affinities of THT to $A\beta(1-40)$ fibrils ranging from 790 nM - 1740 nM.^{33, 34} As to CGR, clustering resulted in many but rather weakly populated clusters, which is not surprising considering the broad distribution of stably bound CGR conformations. We thus primarily focused on the interpretation of the calculated binding affinities to derive a reasonable binding mode. Experimentally derived binding affinities of CGR to $A\beta(1-40)$ range from 48 nM - 1500 nM^{35, 36} and we identified a CGR conformation (Fig. 3D) with $\Delta G_{bind}^0 = -9.78$ kcal mol⁻¹, yielding K_D^{comp} = 74.77 nM. In this conformation, CGR binds to the groove between Y10 and V12. In this pose, the amino groups of CGR form hydrogen bond interactions with the backbone carbonyl oxygen of E11, while the charged and polar phosphate groups are exposed to the solvent (Fig. 3D). The CGR biaryl core forms hydrophobic interactions with Y10 and V12, such that the biaryl core and the Y10 side-chain adopt an edge-to-face configuration. CGR

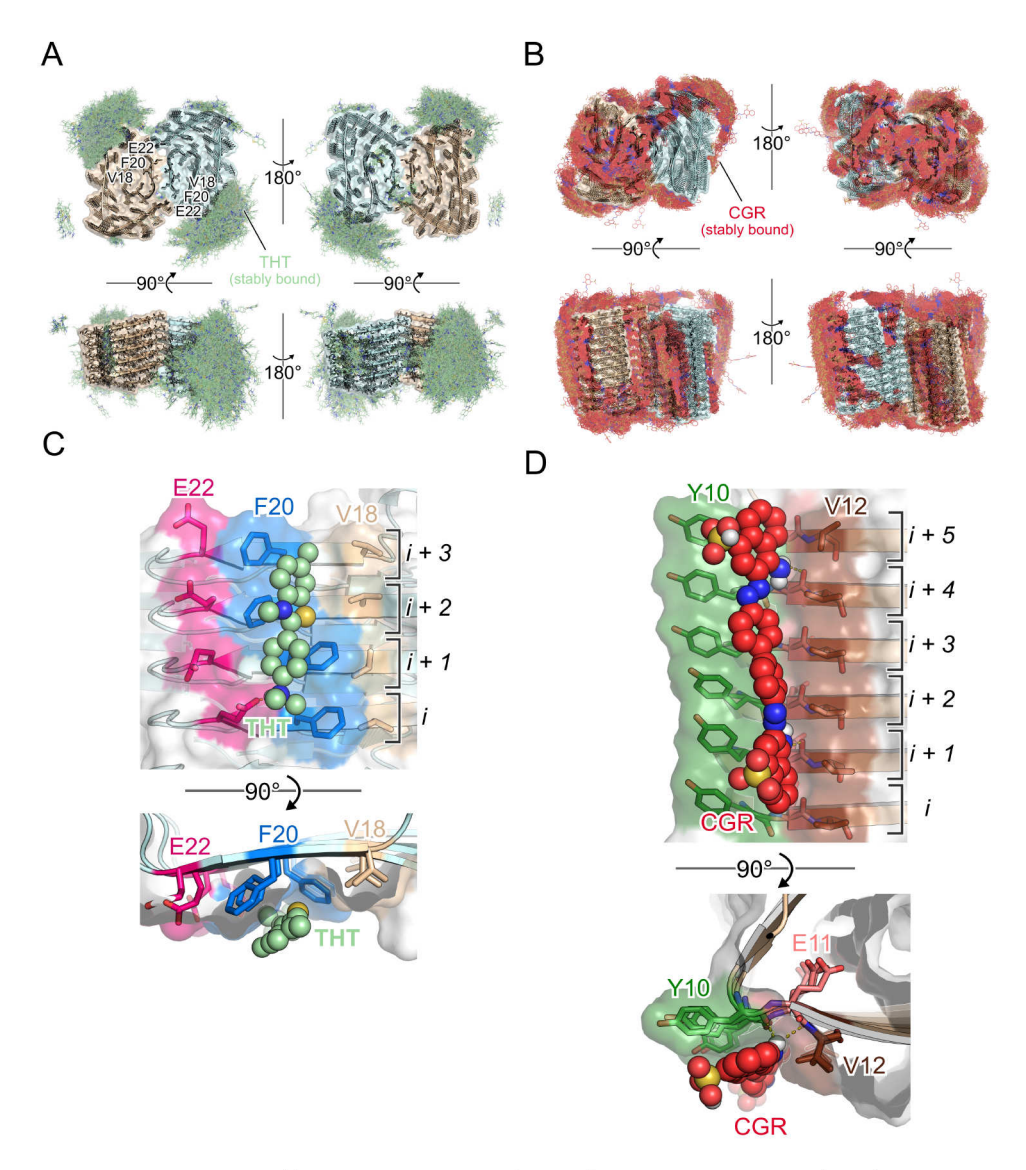


Figure 3. Binding modes of fluorescent dyes at the $A\beta(1-42)$ fibril. A, B: Distribution of Thioflavin-T (THT, A) and Congo red (CGR, B) molecules bound to the $A\beta(1-42)$ fibril. THT is shown as green stick-model and CGR as red stick-model, respectively. The $A\beta(1-42)$ fibril is shown as cartoon-surface representation with each protofibril coloured differently. C, D: Dominant THT (C) and CGR (D) binding poses from side- and top-view shown as sphere models. Amino acids involved in THT or CGR binding are depicted as stick-model.

binds across six layers of $A\beta(1-42)$ peptides with its axis oriented almost perpendicular to the orientation of the stacked β -strands of the $A\beta$ fibril, providing an explanation of why CGR recognises fibrillary structures.

4 Discussion

Binding epitopes and atomistic binding mode models for the fluorescent dyes THT and CGR at the $A\beta(1-42)$ fibril have been identified through unbiased MD simulations and binding free energy calculations. This procedure has been successfully applied to study ligand binding processes before, ^{24, 37–40} also in the field of amyloid research. ^{16, 41}

Our binding mode model suggests that THT likely binds on the surface of the $A\beta(1-42)$ fibril to amino acids V18, F20, and E22, which is in agreement with previous observations on multiple accounts. For example, relative fast binding kinetics of THT binding to fibrils suggests that the dye can easily access its binding site, 42 which can be explained by THT binding to a solvent-exposed surface. Former studies on THT binding to fibrils also suggest a minimal binding site on the fibril surface that covers four consecutive β -strands, 43, 44 a feature we also find for our binding mode of THT (Fig. 3C). THT binds fast and specifically to $A\beta(1-40)$ fibrils, but does not bind to monomers or other oligomeric states, 43 supporting the view that multiple β -strands may be involved in THT binding. THT is reported to bind with its long axis almost parallel to the long axis of the fibrils. 45 This orientation was also observed in an X-ray structure of THT bound to a PSAM ladder, 43 during MD simulations of THT binding to protofibrils forming two-layered β -sheets, 16 and in the present study (Fig. 3C).

As to CGR, our results suggest that it binds on the surface of the $A\beta(1-42)$ fibril to amino acids Y10, E11, and V12, which is in excellent agreement with previous findings. Two structural features are essential for CGR binding to AB aggregates; first, two negative charges that are separated by a fixed distance of 19 Å, 11 and, second, a biaryl core framework. 11 Modifying the gap between the negative charges reduces the binding affinity, 11 while modifying the substituents of the biaryl core does not influence the binding affinity dramatically.^{11, 35} The spacing of 19 Å corresponds to the spacing between five pleated and stacked β -strands,^{12, 17} suggesting that CGR binds across multiple layers, thereby forming ionic interactions. The observation was corroborated by Schütz et al. who showed that CGR binds to the surface of stacked β -strands, thus creating ionic interactions between the sulphonic groups of CGR and lysine residues of the HET fibril.⁴⁶ As the CGR molecule considered in our simulations, however, does not carry two negatively charged groups (Fig. 1B), it is also not surprising that we did not observe the ionic interaction model. Nevertheless, similar to the results from Schütz et al., 46 we find that CGR binds across six layers of Aβ(1-42) peptides (Fig. 3D). In our case, however, the interactions between CGR and the $A\beta(1-42)$ fibril are mainly hydrophobic, which may be explained by a suggested second binding site for CGR-type ligands. 11 For the second binding site, prior studies underline the importance of hydrophobic interactions for CGR binding, ^{12, 16, 47} as some experimental observables cannot be explained by the ionic model.¹¹ Interestingly, for CGR derivatives where no ionic state is expected at physiological pH, the binding affinity is even increased relative to CGR, 11 supporting the view that hydrophobic interactions are crucial for CGR binding. Finally, most studies suggest that CGR binds with its long axis perpendicular to the direction of the β -strands, ^{12, 48} as it was observed in the present study (Fig. 3D).

We validated the binding mode models by comparing computationally derived binding affinities with experimentally derived binding affinities. In general, the binding affinities are in good agreement, although, to the best of our knowledge, there is currently no study available that determined binding affinities for the probes in the presence of the recently

resolved A β (1-42) fibril structure at pH 2.¹⁷ This may be of relevance in the case of THT, as the affinity decreases at acidic pH conditions, suggesting a weak pH dependency for THT binding as observed for THT binding to insulin and HET fibrils. ^{12, 49, 50} As to CGR, there is no evidence suggesting a pH dependency, although most of the affinity studies are done at neutral pH as CGR tends to be insoluble at acidic pH. ¹² In our preparation process of CGR, the p K_a values of the sulphonic acids were predicted ^{18, 19} with p K_a = 2.13 and p K_a = 1.53, such that CGR tends to be in a deprotonated and charged state at pH 2 (Fig. 1B).

In conclusion, we suggest binding sites and binding modes for the fluorescent dyes THT and CGR to the $A\beta(1-42)$ fibril. The binding sites were identified by unbiased MD simulations and subsequently corroborated by calculations of binding affinities. The binding sites and modes agree with previous experimental observations. The binding mode models may provide a starting point for the systematic search and design of novel and improved molecules that bind to $A\beta(1-42)$ fibrils, which is essential for conclusively diagnosing amyloid fibrils-related diseases.

Acknowledgements

The authors gratefully acknowledge fruitful discussion with Lothar Gremer, Henrike Heise, Gunnar Schröder, and Dieter Willbold and the computing time granted by the John von Neumann Institute for Computing (NIC) provided on the supercomputer JUWELS²⁸ at Jülich Supercomputing Centre (JSC) (project ID: HKF7).

References

- 1. J. Wang et al., A systemic view of Alzheimer disease insights from amyloid-beta metabolism beyond the brain, Nat. Rev. Neurol. 13(10), 612–623, 2017.
- 2. P. Scheltens et al., Alzheimer's disease, Lancet 388(10043), 505-517, 2016.
- 3. C. L. Masters et al., Alzheimer's disease, Nat. Rev. Dis. Primers 1, 1–18, 2015.
- 4. H. V. Vinters, *Emerging concepts in Alzheimer's disease*, Annu. Rev. Pathol.: Mech. Dis. **10**, 291–319, 2015.
- 5. Alzheimer's Association, 2019 Alzheimer's disease facts and figures, 2019.
- 6. Alzheimer's Disease International, World Alzheimer Report 2018 The state of the art of dementia research: New frontiers, 2018.
- 7. D. J. Selkoe and J. Hardy, *The amyloid hypothesis of Alzheimer's disease at 25 years*, EMBO Mol. Med. **8(6)**, 595–608, 2016.
- 8. B. A. Gordon *et al.*, Spatial patterns of neuroimaging biomarker change in individuals from families with autosomal dominant Alzheimer's disease: a longitudinal study, Lancet Neurol. **17(3)**, 241–250, 2018.
- 9. M. Goedert et al., The propagation of prion-like protein inclusions in neurodegenerative diseases, Trends. Neurosci. 33(7), 317–325, 2010.
- 10. M. Jucker and L. C. Walker, *Self-propagation of pathogenic protein aggregates in neurodegenerative diseases*, Nature **501(7465)**, 45–51, 2013.
- 11. L. S. Cai et al., Radioligand development for PET imaging of beta-amyloid (Abeta) current status, Curr. Med. Chem. **14(1)**, 19–52, 2007.

- 12. M. Groenning, Binding mode of Thioflavin-T and other molecular probes in the context of amyloid fibrils current status, J. Chem. Biol. **3(1)**, 1–18, 2010.
- 13. A. I. Sulatskaya et al., Interaction of Thioflavin-T with amyloid fibrils: stoichiometry and affinity of dye binding, absorption spectra of bound dye, J. Phys. Chem. B 115(39), 11519–11524, 2011.
- 14. C. Xue et al., Thioflavin T as an amyloid dye: fibril quantification, optimal concentration and effect on aggregation, Roy. Soc. Open Sci. 4(1), 160696, 2017.
- 15. E. I. Yakupova *et al.*, *Congo red and amyloids: history and relationship*, Biosci. Rep. **39**, 1–22, 2019.
- 16. C. Wu et al., Dual binding modes of Congo red to amyloid protofibril surface observed in molecular dynamics simulations, J. Am. Chem. Soc. **129(5)**, 1225–1232, 2007.
- 17. C. Wu et al., Fibril structure of amyloid-beta(1-42) by cryo-electron microscopy, Science **358(6359)**, 116–119, 2017.
- 18. Schrödinger, LLC, Schrödinger Release 2017-3: Schrödinger Suite 2017-3., 2017.
- 19. J. C. Shelley et al., Epik: a software program for pK a prediction and protonation state generation for drug-like molecules, J. Comput. Aided Mol. Des. **21**(12), 681–691, 2007.
- 20. J. C. Shelley et al., PACKMOL: a package for building initial configurations for molecular dynamics simulations, J. of Comp. Chem. **30(13)**, 2157–2164, 2009.
- 21. W. L. Jorgensen *et al.*, *Comparison of simple potential functions for simulating liquid water*, J. Chem. Phys. **79(2)**, 926–935, 1983.
- 22. D. A. Case et al., AMBER 16, University of California, San Francisco, 2016.
- 23. B. Frieg et al., Molecular mechanisms of glutamine synthetase mutations that lead to clinically relevant pathologies, PLoS Comput. Biol. 12(2), e1004693, 2016.
- 24. S. Bhatia et al., Targeting Hsp90 dimerization via the C-terminus is effective in imatinib resistant CML and lacks heat shock response induction, Blood 132(3), 307–320, 2018.
- 25. B. Frieg *et al.*, *Towards restoring catalytic activity of glutamine synthetase with a clinically relevant mutation*, in Proceedings of the NIC Symposium 2016, K. Binder *et al.* (Editors), Jülich, 97–104, 2016.
- 26. T. Darden et al., Particle Mesh Ewald: an N-log (N) method for Ewald sums in large systems, J. Chem. Phys. **98(12)**, 10089–10092, 1993.
- 27. R. Salomon-Ferrer et al., Routine microsecond molecular dynamics simulations with Amber on GPUs. 2. Explicit solvent particle mesh Ewald, J. Chem. Theory. Comput. 9(9), 3878–3888, 2013.
- 28. D. Krause, *JUWELS: Modular Tier-0/1 supercomputer at the Jülich Supercomputing Centre*, JLSRF **5**, A135, 2019.
- 29. B. R. Miller et al., MMPBSA.py: an efficient program for end-state free energy calculations, J. Chem. Theory. Comput. **8(9)**, 3314–3321, 2012.
- 30. S. Genheden and U. Ryde, *The MM/PBSA and MM/GBSA methods to estimate ligand-binding affinities*, Expert Opin. Drug. Dis. **10**(**5**), 449–461, 2015.
- 31. N. Homeyer and H. Gohlke, *Free energy calculations by the molecular mechanics Poisson-Boltzmann surface area method*, Mol. Inf. **31(2)**, 114–122, 2012.
- 32. H. Gohlke et al., Insights into protein-protein binding by binding free energy calculation and free energy decomposition for the Ras-Raf and Ras-RaIGDS complexes, J. Mol. Biol. **330(4)**, 891–913, 2003.

- 33. C. Rodriguez-Rodriguez et al., Thioflavin-based molecular probes for application in Alzheimer's disease: from in silico to in vitro models, Metallomics 7(1), 83–92, 2015.
- 34. R. L. Yona et al., Thioflavin derivatives as markers for amyloid-beta fibrils: Insights into structural features important for high-affinity binding, Chemmedchem **3(1)**, 63–66, 2008.
- 35. W. Zhen et al., Synthesis and amyloid binding properties of rhenium complexes: Preliminary progress toward a reagent for SPECT imaging of Alzheimer's disease brain, J. Med. Chem. **42(15)**, 2805–2815, 1999.
- 36. Y. Wang et al., Synthesis and 11C-labelling of (E, E)-1-(3', 4'-dihydroxystyryl)-4-(3'-methoxy-4'-hydroxystyryl) benzene for PET imaging of amyloid deposits, J. Labelled Compd Radiopharm. **45(8)**, 647–664, 2002.
- 37. G. Martinez-Rosell et al., Molecular-simulation-driven fragment screening for the discovery of new CXCL12 inhibitors, J. Chem. Inf. Model. **58**(3), 683–691, 2018.
- 38. N. Plattner and F. Noé, *Protein conformational plasticity and complex ligand-binding kinetics explored by atomistic simulations and Markov models*, Nat. Commun. **6(7653)**, 1–10, 2017.
- 39. Y. B. Shan *et al.*, *How does a drug molecule find its target binding site?*, Nature Chem. **136(8)**, 3320–3320, 2014.
- 40. H. Gohlke *et al.*, *Binding region of alanopine dehydrogenase predicted by unbiased molecular dynamics simulations of ligand diffusion*, J. Chem. Inf. Model. **53(10)**, 2493–2498, 2013.
- 41. C. König et al., Binding sites for luminescent amyloid biomarkers from non-biased molecular dynamics simulations, Chem. Commun. **136(8)**, 3320–3320, 2018.
- 42. H. LeVine, Stopped-flow kinetics reveal multiple phases of thioflavin T binding to Alzheimer beta(1-40) amyloid fibrils, Arch. Biochem. Biophys. **342(2)**, 306–316, 1997.
- 43. M. Biancalana et al., Molecular mechanism of Thioflavin-T binding to the surface of beta-rich peptide self-assemblies, J. Mol. Biol. **385(4)**, 1052–1063, 2009.
- 44. C. Wu et al., Binding modes of Thioflavin-T to the single-layer beta-sheet of the peptide self-assembly mimics, J. Mol. Biol. **394(4)**, 627–633, 2009.
- 45. M. R. H. Krebs *et al.*, *The binding of thioflavin-T to amyloid fibrils: localisation and implications*, J. Struct. Biol. **149**(1), 30–37, 2005.
- 46. A. K. Schütz et al., The amyloid-congo red interface at atomic resolution, Angew. Chem. Int. Edit. **50(26)**, 5956–5960, 2011.
- 47. J. H. Cooper, Selective amyloid staining as a function of amyloid composition and structure, Lab. Invest. **31**, 232–238, 1974.
- 48. L. W. Jin et al., Imaging linear birefringence and dichroism in cerebral amyloid pathologies, Proc. Natl. Acad. Sci. USA **100**(26), 15294–15298, 2003.
- 49. M. Groenning *et al.*, *Binding mode of Thioflavin T in insulin amyloid fibrils*, J. Struct. Biol. **159(3)**, 483–497, 2007.
- 50. R. Sabaté et al., On the binding of Thioflavin-T to HET-s amyloid fibrils assembled at pH 2, J. Struct. Biol. **162(3)**, 387–396, 2008.